Integrative, Segregative, and Degenerate Harmonics of the Structural Connectome

Benjamin S Sipes, Srikantan S Nagarajan, Ashish Raj

Abstract

Unifying integration and segregation in the brain has been a fundamental puzzle in neuroscience ever since the conception of the "binding problem." Here, we introduce a novel framework that places integration and segregation within a continuum based on a fundamental property of the brain–its structural connectivity graph Laplacian harmonics and a new feature we term the *gap-spectrum*. This framework organizes harmonics into three regimes–integrative, segregative, and degenerate–that together account for various group-level properties. Integrative and segregative harmonics occupy the ends of the continuum, and they share properties such as reproducibility across individuals, stability to perturbation, and involve "bottom-up" sensory networks. Degenerate harmonics are in the middle of the continuum, and they are subject-specific, flexible, and involve "top-down" networks. The proposed framework accommodates inter-subject variation, sensitivity to changes, and structure-function coupling in ways that offer promising avenues for studying development, precision medicine, and treatment response in the brain.

Introduction

A central goal of systems neuroscience is to explain fundamental brain processes shared across individuals. Perhaps the most important fundamental process is the so-called "binding problem," which asks how an *integrated* experience arises from *segregated* sensory information [47]. This philosophical distinction has been established in terms of brain function, where integration and segregation are ends of a continuum from synchrony to asynchrony, respectively [56, 21, 55]. Yet, purely functional accounts cannot explain how this integration-segregation balance emerges from the underlying biological structure. It has been proposed that white matter "structural connectivity" (SC) network topology subserves the integration-segregation balance, with integration originating from the "rich-club" and segregation originating from modularity [59, 54, 16]. However, unlike for function, these separate graph metrics are incommensurable to a single integration-segregation continuum. Furthermore, characterizing what occurs between integration and segregation–the missing-middle–has not received sufficient attention. An integration-segregation continuum based on a fundamental network property is yet to be conceived for structural brain networks.

Understanding how integrative and segregative functional activity arises from SC depends on the "structure-function" relationship of brain networks–often described using graph theoretic and statistical measures [7, 4, 66, 31]. Graph Signal Processing (GSP) extends graph theoretical approaches, providing an elegant and concrete mathematical framework to describe brain function as signal diffusion through the SC [30, 1]. At GSP's heart lies the graph Laplacian matrix and its decomposition into graph *harmonics* (eigenvectors or "gradients" [35]), reflecting orthogonal spatial patterns (wave functions) of a signal in the network, with each harmonic associated with an eigenvalue reflecting its graph frequency [11, 17]. The harmonic decomposition of the graph Laplacian is tantamount to a Fourier Transform; Laplacian harmonics form the Fourier bases that

describe how hypothetical brain signals would "resonate" in the structural network, thereby linking structural graph topology to functional synchrony [30, 40]. Each harmonic is associated with an eigenvalue, and conventionally harmonics are sorted by their ascending eigenvalues.

It is therefore natural to employ the harmonic "eigenspectrum" as the organizing principle for integration and segregation, which may form the continuum we seek. This concept has recently gained currency: lower harmonics have been interpreted as integrative since they capture patterns of *global synchrony*, and higher harmonics have been interpreted as segregative since they capture *local synchrony* [49]. Just as low spatial frequencies in Fourier space represent broad and smooth gradients while high frequencies represent detailed, possibly localized, and noisy patterns, it has been observed that low harmonics reflect the global network structure and hence represent integrative activity while higher harmonics represent segregated network clusters [30, 23, 42, 43]. The lowest harmonics appear to correlate with canonical functional resting-state Networks (RSNs) [62, 65, 3] and were the most effective at predicting functional connectivity (FC) [2, 3]. Accordingly, Preti and Van De Ville [43] suggested dividing harmonics into two classes based on their participation in fMRI: the lowest harmonics were "coupled" to fMRI signal while all higher harmonics were "decoupled." Sometimes these two regimes are also called "illiberal" and "liberal", respectively [30]. Therefore an ascending harmonic eigenvalue ordering is a plausible means of describing the integration-segregation continuum.

However, as we show here, many aspects of the structural harmonics' eigenspectrum make the desired integration-segregation (or "coupled-decoupled") binary problematic and incomplete. The relationship between Laplacian eigenvalues and spatial frequency has only partial mathematical [25] and empirical [23] support. Higher harmonics in particular have been shown to break from strict frequency expectations [23]. Mathematically, graph spectra may be reasonable analogs of spatial frequencies for simpler graphs (e.g., rings and infinite or closed lattices) but not necessarily for complex networks [25, 23], such as the brain [55, 7]. The notion of low harmonics being exclusively coupled to function is also imperfect: higher harmonics also significantly contribute to functional activity, such as in MEG spectra [60, 49] and in alignment with RSNs such as the visual network [62]. Thus, both theoretical and empirical evidence suggests that the coupling-decoupling dichotomy does not neatly align with the integration-segregation continuum.

Can the Laplacian harmonic spectrum serve as an integration-segregation continuum? Do the harmonics follow expectations for the integration-segregation continuum, such as reproducibility across individuals? What fundamental network property could distinguish integrative-versus-segregative harmonics? What represents the "missing-middle" of the continuum, and what is its relevance to the underlying biology and brain function?

In this study, we address these questions using a deep investigation of the structural harmonics' eigenspectrum. First we develop a consensus SC to facilitate an ordering of harmonics across subjects. We seek the most informative ordering of the harmonics that simultaneously addresses the following criteria:

1. The ordering must place integration-like harmonics at one end and segregation-like harmonics at the other.

2. The ordering must reproduce as much as possible notions of spatial smoothness and sparsity.

3. The ordering should be reproducible across individuals in a predictable manner.

4. Harmonics placed similarly along the spectrum must share more properties with each other than those far apart.

We first show that the canonical ordering of harmonics by ascending eigenvalues only partially succeeds in fulfilling the above criteria, but that SC harmonics which deviate from classical Fourier expectations are not reproducible across subjects with this ordering. Then, we show that the above criteria can be met by aligning subject-specific harmonics to the group-level harmonics from the consensus SC (the mean SC across individuals). This new ordering reveals an underlying harmonic reproducibility related to the consensus "gap-spectrum," a fundamental property of the eigenspectrum derived from spectral graph theory. Further, the gap-spectrum naturally partitions the harmonics into three distinct regimes: integrative harmonics have low eigenvalues but high spectral gaps; segregative harmonics have high eigenvalues and high spectral gaps; the "degenerate" harmonics have intermediate eigenvalues but low spectral gaps. The latter regime is so-named in analogy to degenerate modes observed in many physical systems, both classical [53, 18, 36, 28] and quantum [26, 15]. This degenerate regime fills the "missing-middle," has not previously been defined in brain science and is endowed with distinct functional relevance.

Together, the three regimes faithfully account for key group-level harmonic properties including spatial smoothness, sparsity, sensitivity to changes, similarity between individuals, and alignment to functional networks. Hence, a more complete stratification of harmonics requires a trichotomy–integrative, degenerate, segregative–instead of the popular integration/segregation or coupled/decoupled dichotomies. The proposed harmonic trichotomy reveals previously unreported structure-function relationships, explaining resting and task functional networks in a manner that is not possible within prior paradigms.

Methods

Dataset

Data in this study come from the publicly available MICA-MICs dataset of 50 healthy young adults (23 women; mean age 29.54 years) [48]. This dataset was generated with the micapipe connectivity pipeline, and a full description of the image processing steps can be found in their articles [13, 48]. This dataset is not only of high quality, but it features cortical connectivity parcelled in the Schaefer atlas [50] at 10 different spatial resolutions (from 100 to 1000 cortical nodes), with each parcellation including an additional 6 bilateral subcortical regions and the bilateral hippocampus (14 additional nodes total). In addition to using the classical streamline count connectivity (hereafter "SC"), we also analyzed the time series from resting-state functional magnetic resonance imaging (fMRI) scans (TR = 600ms; 695 time points). Most analyses were performed in MATLAB while the Neurosynth analysis was performed in Python.

Connectome Harmonic Analysis

For each subject's SC, we first normalized their SC matrix to a unit Frobenius norm, then we computed the degree normalized Laplacian:

$$L_C = I - D^{-1/2} C D^{-1/2} \tag{1}$$

where I is the identity matrix, D is a diagonal degree matrix of the SC matrix (C). We then computed the eigen-decomposition of the resulting Laplacian matrix.

$$L_C = U \Lambda U^T \tag{2}$$

In (2), U is the orthonormal matrix of harmonic components in each column and Λ is the diagonal matrix of eigenvalues associated with each harmonic.

Harmonic Frequency Analysis

Determining the precise spatial frequency of each harmonic is not straightforward since the brain's harmonic components live in the brain's 3-dimensional space, and a 3D-FFT does not have an obvious single feature representative of the full volume's frequency content. We instead used four measures that relate to spatial frequency and analyzed their relationship to eigenvalues. Since we analyze the harmonic components based on their amplitude, for the below measures we first apply a modest threshold (± 0.001) to eliminate spurious low amplitude fluctuations around zero.

Harmonic Sparsity Harmonic sparsity is measured as the fraction of regions where the harmonic's amplitude is zero. In classical Fourier analysis, the sparsity of all harmonics in a Fourier transform are zero (i.e., all frequencies have infinite support). Therefore, SC harmonics with high sparsity defy Fourier-based intuitions for harmonic components.

Harmonic Zero Cross Rate We used MATLAB's `zerocrossrate` function to measure the rate at which the harmonic component changes polarity, where high frequencies are defined by a high rate of polarity switching oscillations. This measure assumes an ordering of regions such that adjacent regions are also adjacent in the harmonic component. This assumption is generally appropriate, as is clear in the Regional Adjacency matrix that regions close in space are generally adjacent in the regional ordering (Supplemental Material Figure S1).

Harmonic Network Zero Crossings This measure of harmonic frequency was proposed by Huang et al. [23], which accounts for Laplacian harmonics being graph cuts on the network. Network edges between opposite signs in the harmonic are summed to find the weight of the cut. This cut weight can be considered a proxy for the "frequency" of the harmonic with respect to the underlying network since higher frequencies will have less optimal (highly weighted) graph cuts. However, one known difficulty to this approach is that the areas of low harmonic amplitude fluctuate spuriously around zero, and therefore the above threshold is necessary to show graph cuts between regions that meaningfully participate in the harmonic. To see results across thresholds, see Supplemental Material (Figure S2).

Harmonic Spatial Roughness We propose a novel measure for harmonic frequency that accounts for the 3-dimensional adjacency between regions. We term this measure "Spatial Roughness," and it uses a regional adjacency matrix (A), where the entry $A_{i,j}$ is proportional to the number and distance of adjacent shared voxels in MNI space between regions i and j. Our formulation is as follows:

$$\text{Roughness}(u_i) = ||u_i^T L_A|| \tag{3}$$

where L_A is the degree-normalized Laplacian of the regional adjacency matrix (A), u_i is the ith eigenvector of the SC Laplacian, and ($||\cdot||$) is the euclidean norm of the result. Since A is defined only within each hemisphere, we compute the Roughness separately for each hemisphere then average between them. Spatial roughness is high when adjacent regions in the brain are dissimilar

in both their harmonic's signal amplitude and polarity. This high fluctuation in harmonic polarity between adjacent regions is what we would expect from high-frequency harmonic components.

Harmonic Matching

We computed U for each subject's SC individually as well as for a consensus SC, which was formed by taking the average across all subject's networks, by computing the Laplacian (1), then obtaining its eigen-decomposition (2). For each subject, we performed the following algorithm to find an optimal matching between that subject's individual harmonics and those from consensus network harmonics.

Algorithm 1 Match Eigenvectors

function MATCH EIGS($U1, U2$)
  $neigs \leftarrow$ length of $U1$
  $UU \leftarrow$ absolute value of $U1^T \cdot U2$
  $U1_matched \leftarrow neigs \times neigs$ matrix of zeros
  $\sigma \leftarrow neigs \times 1$ vector of zeros
  $missing_eigs, available_eigs \leftarrow$ indices of $U1$
  for $k = 1$ to $neigs$ **do**
    $Rem \leftarrow$ submatrix of UU with rows $available_eigs$ and columns $missing_eigs$
    $[i, j] \leftarrow$ row and column indices of the maximum element of Rem
    $U1_matched(:, missing_eigs(j)) \leftarrow U1(:, available_eigs(i))$
    $\sigma(missing_eigs(j)) \leftarrow available_eigs(i)$
    remove $available_eigs(i)$ from $available_eigs$
    remove $missing_eigs(j)$ from $missing_eigs$
  end for
  return $U1_matched, \sigma$
end function

It is clear from the algorithm that this matching procedure simply identifies a permutation (σ) of columns for an eigenvector matrix (U) that maximizes the diagonal of the projection matrix between two sets of eigenvectors in a winner-take-all fashion. By matching individual subjects to the consensus SC, we retain an ordering of ascending eigenvalues with respect to the consensus SC.

Note that others have recently performed eigenvector alignment using Procrustes [5]; however, we refrained from this approach to preserve as much of the subject-specific features in the harmonics as possible, since understanding the subtle harmonic variation across subjects is a key question evaluated in this work.

Inter-subject Agreement

To evaluate inter-subject agreement between both unmatched and matched harmonics, we computed all possible combinations of subject-specific consensus-matched harmonic component dyads

and took the absolute value of each diagonal.

$$\text{Agreement}(n, m) = |\text{diag}(U_n^T U_m)| \; \forall \; \{n, m\} \text{ subject dyads} \in \binom{50}{2} \tag{4}$$

Note that since these harmonics form orthonormal matrices, subjects with identical harmonic components will have an Agreement equal to 1, and fully orthogonal harmonics will have an Agreement equal to 0.

To find the region-wise inter-subject variability across harmonic components, we first re-scaled subject-specific absolute-valued harmonics so that each was on the closed interval $[0, 1]$, then we took the variance across all subjects followed by the mean across all components.

Eigenvalue Gap-Spectrum

In spectral graph theory, the "spectral gap" of a graph Laplacian is formally defined as the difference between the smallest and second smallest eigenvalues, and it reflects special properties in the network such as indicating overall connectivity. More generally, the "gap" between any two eigenvalues indicates the "degeneracy" between two harmonics, where harmonics with the same eigenvalue (i.e., a gap equal to zero) are considered fully degenerate. Degenerate harmonics are a special class where any linear combination of degenerate harmonics is another degenerate harmonic in the same eigenspace; intuitively, degenerate harmonics can be considered maximally "flexible." Here, we analyzed the SC harmonic eigenspectrum through what we've termed its "gap-spectrum," which is analogous to the derivative of the ascending eigenvalues with respect to their index, and which represents a measure of harmonic degeneracy. To obtain a smooth gap-spectrum for all harmonics, we first fit an order 10 spline with 3 knots to the SC eigenvalues and then computed the first and second analytical spline derivatives as the first and second order gap-spectrum. We hypothesized that the first-order gap-spectrum (measuring harmonic degeneracy) would be related to various properties of harmonic components. We computed the second-order gap-spectrum's maxima and minima to identify transition points in the eigenspectrum that indicate the beginning and ending of the near-degenerate (i.e., flattest) eigenvalue regime.

Stability of Harmonics

We hypothesized that a harmonic's stability to network changes would be related to the gap-spectrum. We perturbed each subject's natural SC matrix by adding a matrix of Rician noise ($\nu = 0$) across a range of σ, then computed its Laplacian harmonics, matched them to the same subject's unperturbed harmonics, and then computed their similarity as the diagonal between them.

$$\text{Similarity}(\sigma) = |\text{diag}(U_\sigma^T U)| \tag{5}$$

Thus, for each σ we obtained a measure of harmonic similarity for every harmonic across subjects. Drawing inspiration from perturbation theory, we define the *stability of harmonics* as the initial slope of decreasing harmonic similarity due to perturbation. We computed the stability of harmonics by fitting a linear slope to the first five σ perturbations, i.e., we approximated the instantaneous rate of change for small perturbations. We compared this stability for each harmonic across subjects to the gap-spectrum.

Harmonic Participation in Function

To investigate how harmonics are related to the brain's function, we define harmonic participation by how known functional resting-state networks, meta-analytic task networks, and empirical resting-state time series align with each harmonic's amplitude gradient. We describe each of these three formulations below.

Alignment with resting-state Networks

Using the Schaefer atlas, each node in the network was labeled according to the 7 canonical resting-state networks [65], with an additional label for the 14 subcortical regions (which we'll consider an unofficial RSN for this analysis). To evaluate harmonic participation with RSNs, we first created a binary matrix Q with eight rows (one row for each RSN) and columns equal to the number of network nodes. We then computed RSN participation for each subject's matched harmonics (U) as

$$\text{RSN Participation} = Q|U|^2. \tag{6}$$

We use $|U|^2$ since this formulation (in analogy to the"Born rule") is most appropriate for analyzing harmonics as synchronizing wave amplitude distributions. In other words, we ignore harmonic polarity and emphasize harmonic amplitude such that a given harmonic participates with an RSN if its amplitude localizes to that RSN. We are most interested in the relative participation between various RSNs, so we row-normalize the RSN Participation matrix by the maximum value in each RSN. For the participation without row-normalization, see Supplemental Material (Figure S3).

Alignment with Meta-analytic Task Networks

To evaluate the correlation between SC harmonics with meta-analysis task activation maps, we exported the Born rule harmonics ($|U|^2$) from the 214 node network for each subject into NIFTI files in MNI space. We then used the `NiMARE` toolbox in Python to compute the correlation between the eigenvectors and Neurosynth task activation maps for 146 Latent Dirichlet Allocation (LDA) topics drawn from the LDA-400 set (Neurosynth version-7). We included topics related to cognitive processes while we excluded topics related to methodology or clinical conditions. We then averaged subsets of the 146 topic terms to obtain 24 separate cognitive domains similar to those applied in previous meta-analysis studies using Neurosynth [35, 43]. (For a full list of LDA terms and their cognitive domain assignments, see Supplemental Material Table 1.)

We used ternary plots to analyze the relative contribution of harmonic components for both RSNs and task activation correlations. To limit the influence of spurious correlations in this analysis, we applied an 80th percentile thresholded (across all subjects) to both the RSN participation strength and Neurosynth correlations, we then averaged across subjects to obtain group-level harmonic participation maps.

Harmonic participation in resting-state fMRI time series

Finally, we projected the empirical resting-state fMRI time series into the harmonic space and analyzed their properties. This projection follows a similar procedure as previous works [38, 43, 3, 33], but we instead use the Born rule harmonics ($|U|^2$), which is aligned with our aim to understand

harmonics' synchrony in the brain. Given a time series ($S(t) \in \mathbb{R}^{\text{time x region}}$), the projection becomes:

$$\hat{S}(t) = S(t)|U|^2. \tag{7}$$

To study the functional properties of the harmonic signals, we analyzed the signal energy, sample entropy, harmonic diversity, and temporal dynamics.

The energy of a signal ($\hat{s}_i(t)$) is defined as the L-2 norm across time. We computed the energy for each harmonic projection to compare across the different harmonic regimes. We further assessed the regional distribution of harmonic energy by projecting the energy back into the region space. We computed the sample entropy for each individual harmonic, then averaged across each harmonic regime to compute the bits per harmonic each regime contained. We similarly computed harmonic diversity, which measured how much the functional signal was balanced across multiple harmonics (analogous to the measure introduced in [33]). Since this measure is influenced by the number of harmonics in a given regime, we normalized by the maximum possible diversity for each regime. Finally, we analyzed the dynamics of harmonics by constructing a relative phase-space representing the brain's participation in each harmonic regime. We characterized the dynamics in this space by the mean location the brain occupied as well as the first principle component to show the main axis of dynamic fluctuation.

Results

Here, we present results from analyzing group-level properties of SC harmonics that investigate the integration-segregation continuum. We begin by showing that harmonics deviate from strictly ascending frequencies and have an integration-segregation like structure. We then show that integrative and segregative harmonics are shared across individuals, as would be predicted by the binding problem. Then, using the gap-spectrum, we define integrative, segregative, and *degenerate* regimes precisely, and confirm that it accounts for previously described properties. We conclude by investigating the functional relevance of the three regimes in multiple ways, including stability to changes, alignment with resting-state networks, task networks, and empirical resting-state data.

SC harmonics do not directly correspond to spatial frequency

Qualitatively, we found that the lowest harmonics in the consensus SC matched with those previously reported [61, 33, 5] (Figure 1A). Quantitatively, we investigated how SC harmonics related to spatial frequency properties; namely sparsity, zero-cross rate, network zero-crossings [23], and roughness. Across all measures, the highest harmonics' eigenvalues deviate from classical notions of frequency: they have high sparsity, and they have decreased zero-cross rates, network zero-crossing connectivity, and spatial roughness. We further observed that the notable change in these measures generally happened for harmonics with eigenvalues $\lambda \geq 1$. For completeness, we also analyze harmonics' temporal frequency when projected onto empirical resting-state time series (Supplemental Material Figure S4), finding that again that higher harmonics are not necessarily related to higher frequency in fMRI.

Taken together, we find only partial support that SC Laplacian eigenvalues correspond to spatial frequency. While there is undoubtedly some relationship, it is far from monotonic, and it suggests that harmonics organized by ascending eigenvalues across subjects could be misaligned.

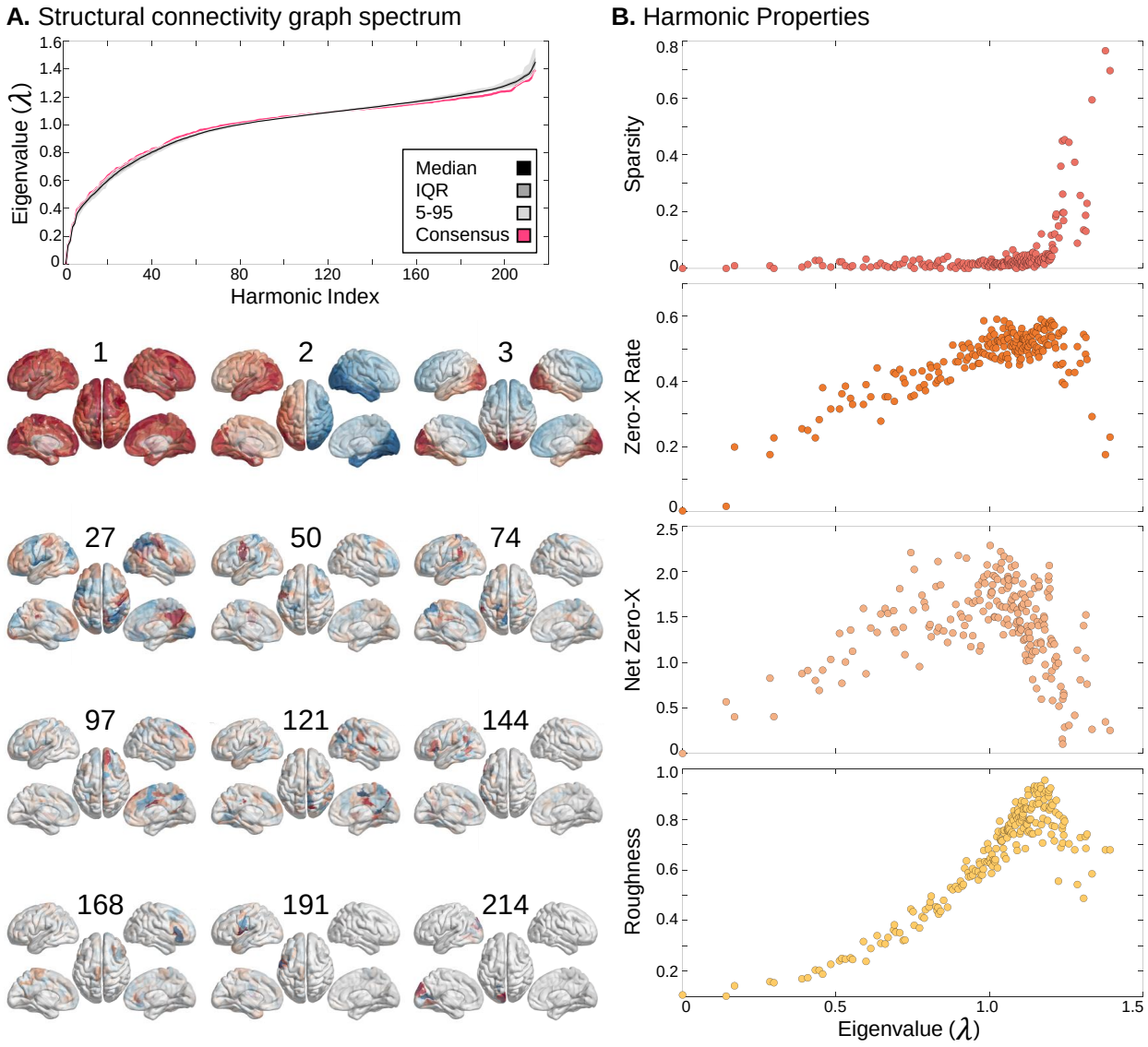

Figure 1: **SC Harmonic Spectrum.** (A) On top, we show the Laplacian eigenvalue spectrum for the SC network with 214 regions. In rose is the eigenvalue spectrum from the consensus (group-averaged) SC, and overlain on top in black is the median eigenvalue spectrum across all 50 subjects with shaded group percentiles. Below the eigenvalues we show several harmonics from the consensus SC with their harmonic index labeled above each plot. Notice that the harmonics become sparse and localized as eigenvalues increase. (B) We show four properties of the consensus SC harmonics: (top to bottom) sparsity, zero crossing rate, network zero crossings, and spatial roughness. The highest eigenvalue harmonics are distinct across all features.

Matching subjects to consensus harmonics reveals inter-subject similarity

Next, we used a measure of inter-subject agreement (4) to test whether subjects had similar harmonics for both whole-brain (integrative) and sparse (segregative) ends of the eigenspectrum. When all subjects' harmonics are sorted by their ascending eigenvalues, we only observe strong agreement for the first few harmonics (Figure 2 A & B). We then matched subjects' harmonics to those from the consensus SC in a winner-take-all fashion (1), which revealed that many subjects indeed shared harmonics at both ends of the consensus eigenspectrum (Figure 2 C & D).

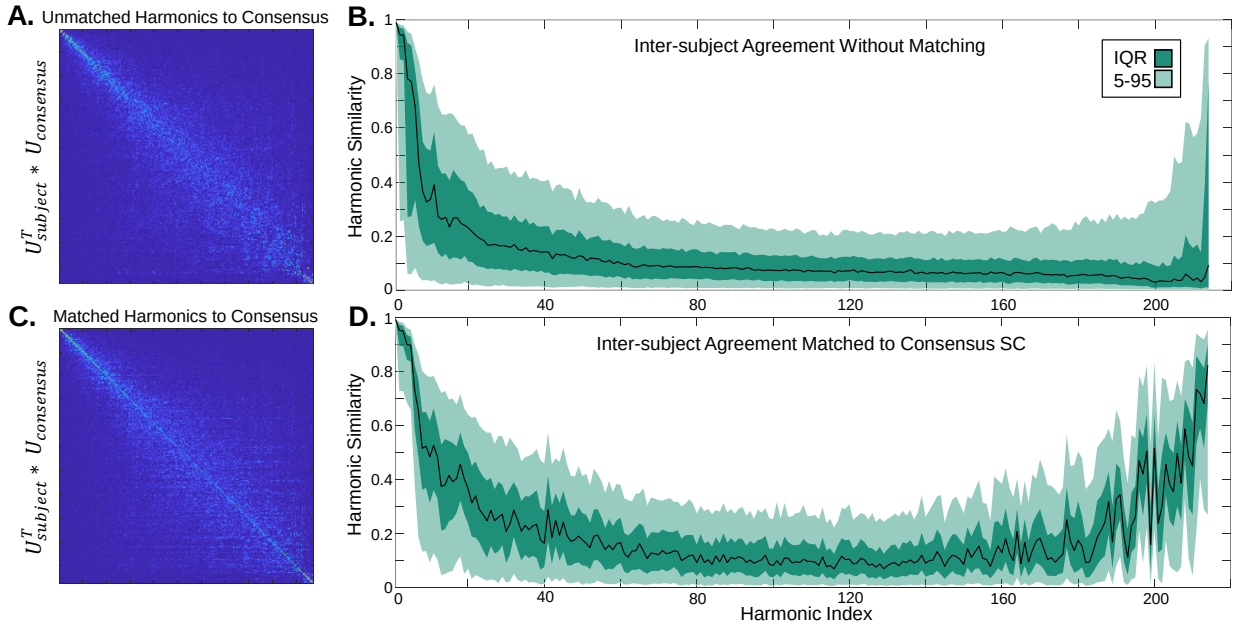

Figure 2: **Harmonic Inter-subject Agreement.** (A) Harmonics do not show a natural alignment to the consensus SC, and (B) inter-subject agreement, measured as the harmonic similarity across all combinations of subjects, showed that most subjects are misaligned for most harmonics. But (C) matching harmonics can maximize this similarity on the diagonal, and (D) following harmonic matching, we observe that subjects share many of the same lowest and highest harmonics. In B & C, the black line indicates the median, while the shaded regions indicate the interquartile range (IQR; darker) and 5th to 95th percentiles (lighter).

We found this result to be consistent across all Schaefer parcellations (Supplemental Figure S5). Furthermore, we evaluated the Bonferroni corrected significance between the two agreement distributions and found that nearly all harmonics showed highly significant agreement improvement after matching (Supplemental Figure S5). We then generated null-model networks with randomized edge weights from empirical SC networks and found that these randomized networks were unable to match. Empirical matching showed highly significant agreement compared to randomized harmonics (Supplemental Figure S6).

To better understand harmonic misalignment, we computed the permutation length (defined as the number of column switches) for each harmonic across subjects, finding that the central harmonics required the longest permutations to match to the consensus ordering (Supplemental Figure S7). We also computed the Kendall's Tau (KT) correlation, which is a measure of total permutation distance, for each subject with respect to the consensus SC (Supplemental Figure S7), finding that overall subjects showed a harmonic ordering similar to the consensus SC (mean(std) KT = 0.88(0.02)).

We next examined which harmonics were most variable across subjects. We found that the highest harmonics were the least variable between subjects compared to other harmonics ($p << 0.001$; Supplemental Figure S8). There was a general negative relationship between harmonic variation and mean inter-subject agreement ($r = -0.47; p << 0.001$; Supplemental Figure S8). We further found that the least harmonic variation across subjects were in the visual, somatomotor, auditory, and limbic areas (Supplemental Figure S8). Unexpectedly, the orbitofrontal cortex also showed low inter-subject harmonic variation. The areas with the greatest inter-subject varia-

tion were trans-modal functional network regions such as the bilateral parietal cortex and lateral prefrontal cortex (Supplemental Figure S8).

Eigenvalue gap-spectrum as a theoretical explanation for harmonic properties

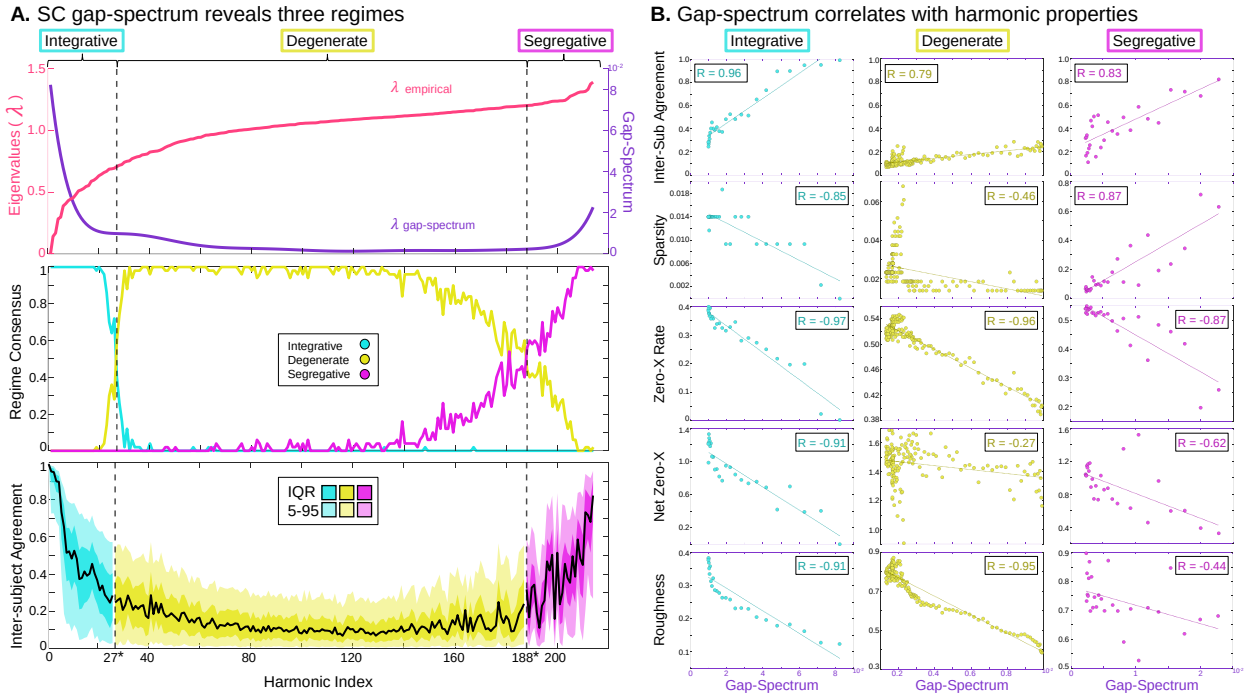

Figure 3: **Defining Three Harmonic Regimes.** (A) We show the consensus SC Laplacian eigenspectrum in rose and the analytical gap-spectrum in violet. We used the maxima and minima of the second-order gap-spectrum (shown in Supplemental Material Figure S9) to find curvature transition points in the natural eigenspectrum for each subject. Below this plot, we show the fraction of subjects who agree on each harmonic regime assignment. (See Supplemental Material Figure S10 for relationship between subject-specific versus consensus eigenvalues and gap-spectrum.) We define the final regime boundaries based on the majority crossing point. The lowest panel shows inter-subject agreement colored by the three regimes. (B) We show the population median values for the four harmonic frequency measures compared to the gap-spectrum. All measures show strong and significant correlations within the identified regimes and the gap-spectrum.

The harmonic inter-subject similarity analysis suggests there are at least three kinds of harmonics: those with low eigenvalues and high inter-subject agreement, those with high eigenvalues and high inter-subject agreement, and those with eigenvalues near $\lambda = 1$ and low inter-subject agreement. In spectral graph theory, the "gap" between two harmonics' eigenvalues quantifies how much unique information about the network is contained between harmonics–larger gaps indicate distinct network configurations while smaller gaps indicate similar network configurations (Figure 3A top). We therefore hypothesized that change-points in the "gap-spectrum" curvature (see Methods) would naturally partition harmonics into regimes that follow the empirical relationship with inter-subject agreement while preserving relationships with harmonic frequency. We first found regime transition points for each subject individually, then we matched subject-level harmonics to

the consensus SC, and finally we determined a consensus regime assignment (Figure 3A middle). We found the lowest regime to span harmonic 1 to 26, the central regime to span harmonic 27 to 187, and the highest regime to span 188 to 214.

Our results support the hypothesis that the gap-spectrum across subjects can indeed partition harmonic inter-subject agreement in an intuitive fashion while preserving relationships to group-level harmonic frequency (Figure 3B; all $p < 0.05$). Based on our harmonic frequency analysis, we term the lowest regime as *integrative* since these harmonics show low-frequency whole-brain spatial configurations. We term the middle regime as *degenerate* since the gap-spectrum is small for these harmonics. Finally, we term the highest regime *segregative* since these harmonics form dense regional clusters.

Stability of harmonics relates to the gap-spectrum

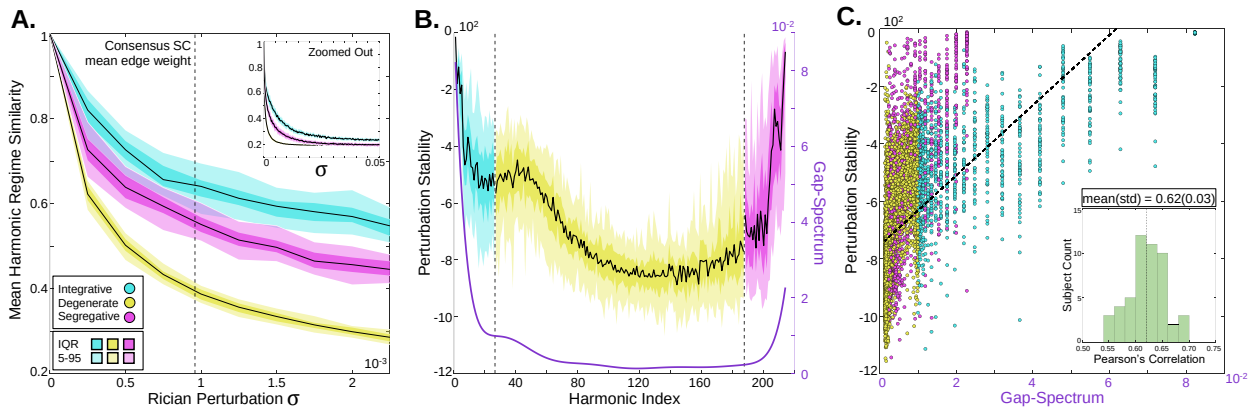

Figure 4: **Stability of Harmonics.** We perturbed the natural SC network across subjects with Rician noise over a wide range of sigma. (A) We plot each regime-averaged intra-subject similarity between the authentic harmonics and the perturbed harmonics. The black line represents the median, while the darker and lighter shaded regions represent the IQR and 5-95 percentile range, respectively. Integrative harmonics show the most stability, segregative harmonics show intermediate stability, and degenerate harmonics show the least stability. The inset shows the same perturbation effect, but over a wider range of σ. (B) We quantify the stability of each harmonic and show that the stability follows the same general shape as the consensus gap-spectrum. (C) A scatter plot with data from all subjects and all harmonics, showing the overall relationship between the stability of harmonics and the gap-spectrum. The inset shows the distribution of subject-specific correlations between the stability of harmonics and gap-spectrum.

We next sought to characterize functionally relevant aspects of the integrative, segregative, and degenerate regimes. One especially meaningful biological dimension to SC is how network changes influences harmonics.

Degenerate harmonics with eigenvalues close to $\lambda = 1$ represent recurring network configurations (or "motifs") [14], and they have mathematical "flexibility" because linear combinations of degenerate harmonics can produce another degenerate harmonic in the same eigen-subspace. Based on this theory, we hypothesized that degenerate harmonics would be sensitive to perturbation, since small perturbations could easily change the network's motif structure.

To test this hypothesis, we simulated white matter rewiring by perturbing each subject's SC with a matrix of random weights drawn from a Rician distribution ($\nu = 0$) with increasing σ. For each value of σ, we measured the perturbation similarity as the diagonal between each subject's

native (matched) harmonics and those after the perturbation. We found that degenerate harmonics were the most sensitive to perturbation while integrative and segregative harmonics were more stable (Figure 4A). As perturbation σ increased far beyond the mean network weight, we found that all regimes approximated an exponential decay (Figure 4A inset).

To quantify the stability of harmonics, we found the initial linear slope of the harmonic similarity, where the change is greatest. Stability of harmonics indeed followed the same shape as the gap-spectrum (Figure 4B). The stability of harmonics across subjects was significantly correlated with the consensus gap-spectrum ($p << 0.001$; Figure 4C).

Harmonics have diverse participation in RSNs and functional tasks

Another meaningful functional aspect of SC harmonics is their alignment with known functional organizations during rest and tasks. We next hypothesized that canonical resting-state functional networks (RSNs; [65]) and meta-analysis task activation maps would show distinct relationships to different harmonic regimes. We computed the RSN participation matrix for each subject after harmonic matching, then we averaged across subjects and normalized by the maximum participation of each RSN. We used an analogous approach with the `NiMARE` toolbox and the Neurosynth database (version 7) to measure the mean correlation for 24 general cognitive domains and each harmonic (see Methods).

We found that SC harmonics relate to RSNs across the eigenspectrum, and RSNs show regime specificity across subjects (Figure 5A&C). The ternary plot showed that the Control Network and the Salience Ventral Attention Network participated most in the degenerate regime; the Subcortex, Visual, and Limbic Networks participated most in the segregative regime; the Somatomotor and Dorsal Attention Networks participated in a balance of the degenerate and segregative regimes; and the Default Mode Network had a balanced mixture of all three regimes (Figure 5C). RSN participation followed a similar relationship across Schaefer parcellations (Supplemental Material Figure S5). We further found that whole brain task activation maps correlated with SC harmonics (Figure 5B). The ternary plot showed that tasks also had differential participation in all three harmonic regimes (Figure 5D). For example, Prediction and Learning was mostly integrative, while Inhibition was mostly degenerate, and Emotion was mostly segregative. Most cognitive tasks involved a balance of the three regimes, such as Language and Decision Making, having approximately 50% integration, and between 20-30% degenerate and segregation.

Harmonic functional activity is different across regimes

Having found a relationship between harmonic regimes and known functional organizations, we hypothesized that empirical resting-state activity would also show similar regime-specific differences and relative regime contributions. We evaluated the functional characteristics of the three regimes in resting-state fMRI data by projecting SC harmonics onto the fMRI time series, thereby obtaining a new time series in the harmonic space (Figure 6 A).

We quantified three key properties of the functional projection: projection energy, temporal diversity, and spatial diversity. The regime projection energy (L-2 norm across time) gradually decreases from low to high harmonics with no clear demarcation between regimes (Figure 6 B). The blue triangle indicates the previously reported divide between coupled/decoupled harmonics based on the reported eigenvalue [43]; this showed that the previously identified uncoupled

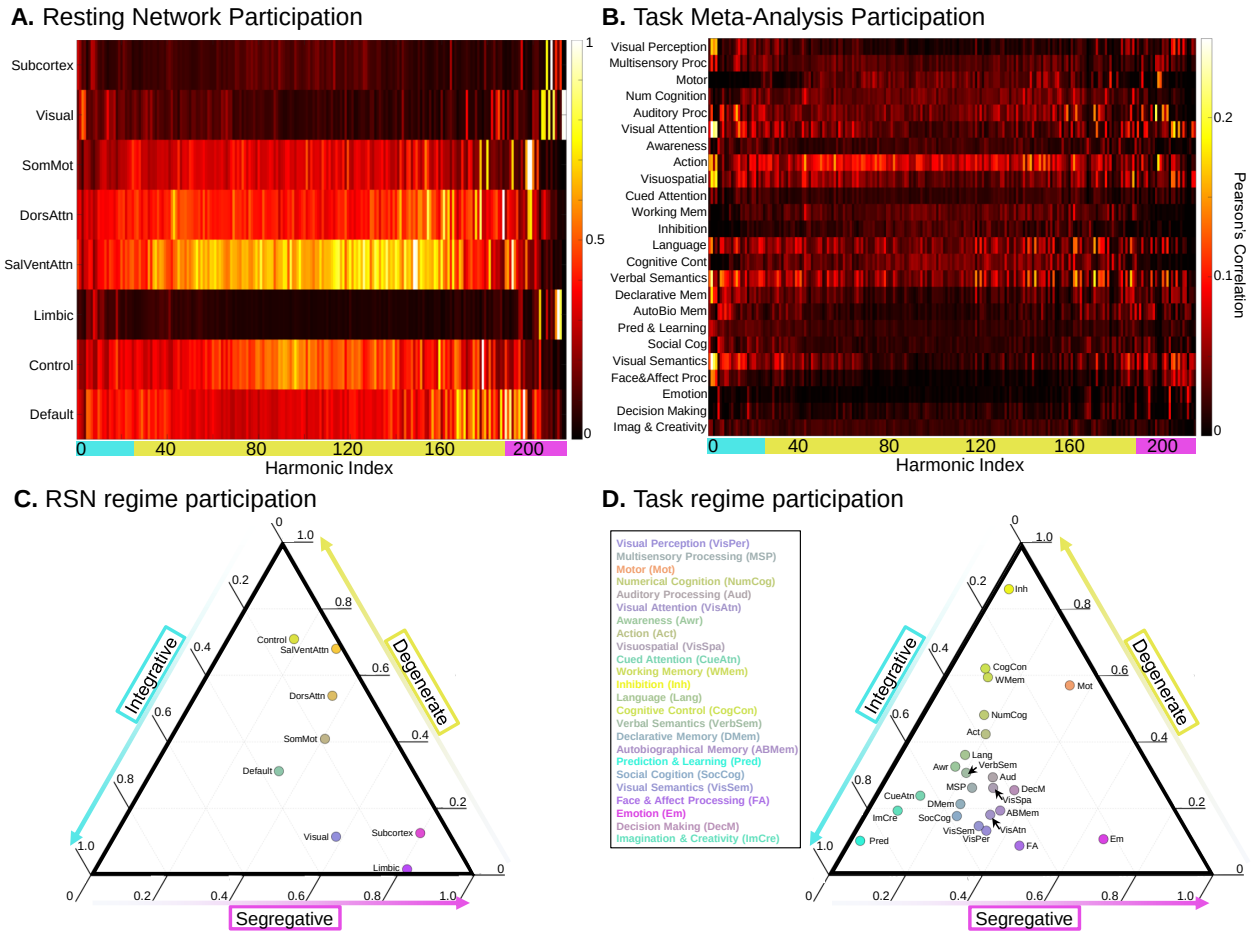

Figure 5: **RSN and Neurosynth Coupling.** We evaluated which harmonics had spatial organization that coupled with (A) resting-state functional networks (RSNs) and (B) Neurosynth task activation maps. All harmonics show spatial patterns that aligned with known functional organization. Below (C & D), we show ternary plots representing the above heat-maps as relative mixtures of each regime's participation in (C) RSNs and (D) Neurosynth task activation networks. Note that the vertices of a ternary plot represent full participation in the respective regime, and the axis ticks are slanted to indicate the direction of the axis along dashed lines. Note that the DMN, for example, is nearly at the center of the RSN ternary plot, meaning it has close to equal participation from all three regimes. Conversely, the Limbic network showed almost exclusive participation in the segregative regime. The bubbles inside the ternary plot are colored based on their proximity to each of the three vertices (cyan–integrative; yellow–degenerate; magenta–segregative).

regime is partially within our integrative regime and entirely within the degenerate and segregative regimes. Quantifying the spatial energy distribution across brain regions showed that integrative harmonics had a broad and relatively homogeneous energy distribution across the cortex, but with an energy peaks located in sensory cortices; degenerate harmonics had energy weighted highest in frontopariteal and inferior temporal lobes; and segregative harmonics had sparse energy, with clusters of high energy in sensory regions, temporal poles, and ventromedial/orbitofrontal cortices (Figure 6 C). Overall, each regime had significantly different energies, with integrative having the most, segregative having the least, and degenerate in-between (all $p << 0.001$; Figure 6 D).

We analyzed temporal diversity (sample entropy) and spatial diversity (harmonic entropy) across regimes. The average temporal diversity contained in each harmonic regime projection

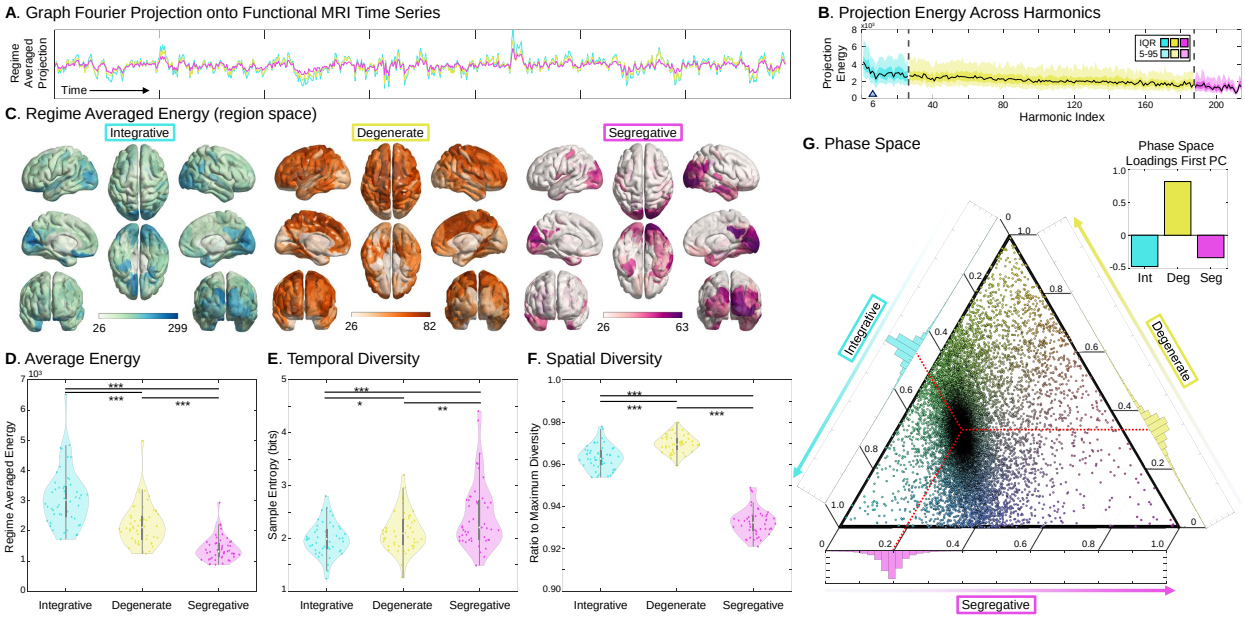

Figure 6: **fMRI Projection.** (A) We project the SC harmonics onto resting-state functional MRI time series and show the regime-averaged projection for a single subject. (B) The projection energy (L-2 norm across time) across all SC harmonics. The blue triangle indicates the previously reported divide between coupled/decoupled harmonics [43]. (C) The projection energy is mapped back to region space, showing region-wise resting-state functional participation in each regime. (D) Quantifying the regime-wise projection energy showed that the integrative harmonics have the most energy per harmonic, followed by the degenerate harmonics, and least for the segregative harmonics. (E) Quantifying the harmonic signal's temporal diversity)(i.e., sample entropy) showed the opposite pattern, with segregative harmonics carrying the most bits per harmonic, followed by degenerate and integrative regimes. (F) Quantifying the diversity of each regime in the functional time series showed that many degenerate harmonics are co-active, while integrative and segregative harmonics are more specific in time. (G) We construct a ternary plot phase space, showing that the brain spends most of its time in a state of 50% integration, 30% degenerate, and 20% segregation. The upper-right inset shows the first principal component of this distribution, indicating that most functional variation is along the degenerate axis.

showed that the segregative harmonics contained the most temporal diversity compared to either integrative or degenerate regimes ($p < 0.005$; Figure 6 E). Degenerate harmonics also had significantly more temporal diversity compared to integrative harmonics ($p < 0.05$). We analyzed harmonic spatial diversity, which measures the entropy of harmonic co-activation at each time-point and then averaged across time. Importantly, we normalized by the maximum possible diversity per regime, since more harmonics in a regime will naturally result in more harmonic diversity. Regimes showed significantly different spatial diversity, with the degenerate regime having the most diversity, followed by the integrative regime, and least in the segregative regime (all $p << 0.001$; Figure 6 F).

Finally, we analyzed how the resting-state brain traversed the 3-dimensional regime phase-space. We found that resting-state function across subjects moved throughout the entire phase-space, but had a strong tendency to be around approximately 46.5% integrative, 33.6% degenerate, and 19.9% segregative (Figure 6 G). Decomposing the trajectory with principal component analysis, we found that the degenerate regime formed the principle axis of temporal variation (Figure 6 G inset).

Discussion

In this work, we have shown that an integration-segregation continuum in SC can be identified through its graph Laplacian harmonics and a novel feature we call the "gap-spectrum." The gap-spectrum represents a fundamental feature of SC that naturally divides harmonics into three regimes: integrative, segregative and degenerate. This harmonic trichotomy reveals distinct regime-specific roles for inter-subject agreement, stability of harmonics, and functional relevance. As we discuss below, this proposed integration-segregation continuum subsumes, refines, and expands upon prior work on SC and its harmonics, affirming those results while recasting the scientific explanations in light of the SC gap-spectrum and the harmonic trichotomy.

Prior work on SC harmonics has focused on a narrow band of the lowest eigenvalue harmonics [2, 35, 3], while other work has attempted to classify all SC harmonics into two categories based on their participation in resting-state fMRI time series [43]. While both approaches have deepened our understanding of SC harmonics, they also possess limitations. Analyzing only the lowest harmonics potentially discards functionally relevant signal contained in the higher harmonics. Meanwhile, classifying harmonics based on their functional participation means their functional relevance is entangled with their classification. The SC gap-spectrum, being both well-defined for all harmonics and inherent to SC, classifies harmonics while avoiding these limitations.

Prior work has emphasized SC Laplacian eigenvalues as reflecting harmonic "spatial frequency" [30, 3, 33]. However, we have shown that measures of the harmonics' spatial frequency are not directly related to their eigenvalues (Figure 1), a finding which has been alluded to in past work [23, 43]. Similarly, work on structure-function relationships has described harmonics as either low-frequency and "coupled" with function or high-frequency and "decoupled" (or "liberal") with function [43, 30, 24]. This coupled-decoupled framework has proven useful, demonstrating relationships with the mechanics of cognition and behavior [43, 32, 6, 67] and serving as a bio-markers of development [19, 39] and disease [63, 68]. Our results affirm the success of the "coupling" versus "decoupling" work while additionally suggesting a further refinement into the integrative, degenerate, and segregative trichotomy. We emphasize that all harmonics "couple" with function in diverse ways related to the harmonic regime.

The brain's function across many representations–RSNs, tasks, and empirical resting-state activity–can be understood under this refined framework as a balance of integrative, segregative, and degenerate harmonics, each with distinct characteristics. Interestingly, the only functional network to show a near-perfect balance of the three regimes is the DMN. We speculate that this is related to the DMN's position at the top of the functional hierarchy [35], and by mixing all regimes, the DMN may allow for easy transitioning to diverse brain states. Other RSNs and all tasks show preferential use of certain harmonic regimes. Functions related to sensation, sociality, and memory were balanced between integrative and segregative harmonics. Conversely, degenerate harmonics were related to complex "top-down" cognition, such as attention, inhibition, and working memory.

The proposed framework places integration and segregation on a single continuum, the SC Laplacian eigenspectrum, which has demonstrated empirical and theoretical relationships to functional activity both in the present and in past work [2, 30, 60, 43]. Since SC harmonics reflect patterns of synchrony in the brain [40], this serves as an elegant compliment to the functional definition of integration and segregation [56]. The proposed integration-segregation continuum also overcomes a present limitation that network hubs in the "rich-club" can only integrate in time, not in space [37], both of which is necessary to resolve the binding problem. We suggest that SC

harmonics represent a parsimonious explanation for the emergence of both spatial and temporal integration in the brain.

The binding problem seeks to explain how the brain can bind segregated sensory channels into an integrated whole. It is known that sensory cortices are generally more segregated from the rest of the brain compared to other regions [51, 52], and yet some balance of integration and segregation must be necessary to bring all senses into a single coherent precept [57]. We observed that both integrative and segregative harmonics relate to sensory "bottom-up" processing, suggesting that this framework may offer plausible solutions to the binding problem. In particular, we found that sensory tasks–visual, spatial, auditory, and multi-sensory processing–are represented across subjects by features in both integrative and segregative harmonics, just as the binding problem would predict. Furthermore, when analyzing the projection of SC harmonics onto fMRI time series, we find again that both integrative and segregative harmonics show remarkably symmetric regional participation across the cortex with greatest strength in the unimodal/sensory regions. Yet these two regimes also have distinct functions–segregative harmonics have more resting-state temporal diversity compared to integrative harmonics, reflecting a potentially synergistic relationship for processing sense data in the brain. We further speculate that segregative harmonics "resonate" with a variety of incoming data, and their overlap with integrative harmonics activates them in turn to broadcast the newly "bound" information globally.

Another implication for this framework is a natural definition for the center of the integration-segregation continuum: the degenerate harmonics. Degenerate harmonics have the greatest resting-state dynamical spatial diversity of any regime, meaning that a wide range of degenerate harmonics contribute to functional activity. These results are aligned with recent work on the dynamics of "decoupled" FC [44], except we show that this may not be true for all "high frequency" harmonics, only for those with a small gap-spectrum. In isolation, any single degenerate harmonic may appear "decoupled" from known functional activity, yet it is their collective activity, resonating in dynamic and flexible combinations, that determine their functional significance.

Defining the degenerate harmonics separate from the integrative and segregative regimes reveals a new subspace of SC related to both individual variation and sensitivity to network changes. This result has the potential to advance precision medicine, since it can disentangle common vs idiosyncratic brain features in a mathematically principled and biologically revealing manner. Progress in this direction has generally been made through research on "brain fingerprinting," which has highlighted the frontal and parietal cortices as those contributing to subject uniqueness [20, 34, 58, 46, 27, 10, 9, 64, 41, 12, 29] and neural plasticity [64]–the same brain regions we found over-represented in the degenerate harmonics. Most promisingly, Griffa et al. [22] has shown that FC filtered by "decoupled" SC harmonics (mostly the degenerate regime) contains highly unique features in the frontoparietal networks useful for brain fingerprinting. This tendency to be subject-specific may be related to degenerate harmonics' sensitivity to subtle network changes, since as humans develop, it could be expected that the SC network will naturally differentiate in increasingly subtle ways for each individual. Degenerate harmonics being flexible in this way also makes them an ideal substrate for neural plasticity when considering the brain's frugal metabolic [8] and wiring cost [45] economy. These results together raise exciting possibilities for future work to compute a reduced SC that isolates the degenerate harmonics, allowing precise investigations of individual uniqueness and neuroplasticity.

These promising advances must be balanced with known limitations for SC harmonics. Noise, low resolution and artifacts are common in diffusion MRI. Tractography algorithms and their as-

sociated parameters can greatly affect quality of tracts, including choice of edge weights, turning angle, stopping criteria, etc. These can have significant effects on connectome quality. While many prior studies have generally identified similar harmonics as shown here [61, 30, 5], the degenerate regime may be particularly affected by these choices. Another limitation is our use of the consensus SC which was constructed from a cohort of 50 healthy young adult subjects. Future work will benefit from constructing a consensus SC with larger healthy samples, and it is presently unclear whether our findings would extend to clinical or developmental populations. With respect to our Neurosynth meta-analysis, the Neurosynth topic terms presented here were averaged across the LDA-400 list where we selected the 146 terms related to cognitive (but not illness or methodological) terms. We chose these to maximize similarity to previously published work related to SC and functional network harmonics [35, 43]. We believed that averaging correlations across many LDA terms and subjects would be more likely to eliminate findings rather than cause spurious results. Finally, we want to acknowledge an inherent tension between presenting SC harmonics as an integration-segregation continuum while also defining three discrete regimes of that continuum. The three regimes depends entirely on defining the criteria for the regimes' cut-off. We show that defining regimes based on the gap-spectrum provides one way to distinguish different properties of SC harmonics, but this need not be the only effective method. Future work using Laplacian harmonics to study integration and segregation in the brain should define these regimes to fit the context of the particular scientific question being asked.

Ultimately, unifying integration and segregation into a single continuum is crucial to understanding systems-level processing in the brain. We propose a framework for this unification based on the "gap-spectrum," which we show can account for an integration-segregation continuum along with a previously undefined center we term the "degenerate" harmonics. The proposed trichotomy of graph harmonics reveals previously unreported structure-function relationships in a manner that is not possible within the integration/segregation nor coupled/decoupled paradigms. This finding provides key biological and functional interpretations for structural brain harmonics, bringing network neuroscience closer to precision medicine and a framework to solve the age-old binding problem.

References

[1] F. Abdelnour, H. U. Voss, and A. Raj. Network diffusion accurately models the relationship between structural and functional brain connectivity networks. *NeuroImage*, 90:335–347, 2014. ISSN 1053-8119. doi: https://doi.org/10.1016/j.neuroimage.2013.12.039. URL https://www.sciencedirect.com/science/article/pii/S1053811913012597.

[2] F. Abdelnour, M. Dayan, O. Devinsky, T. Thesen, and A. Raj. Functional brain connectivity is predictable from anatomic network's Laplacian eigen-structure. *NeuroImage*, 172:728–739, 2018. ISSN 1053-8119. doi: https://doi.org/10.1016/j.neuroimage.2018.02.016. URL https://www.sciencedirect.com/science/article/pii/S1053811918301046.

[3] S. Atasoy, I. Donnelly, and J. Pearson. Human brain networks function in connectome-specific harmonic waves. *Nature Communications*, 7:10340, 2016.

[4] D. S. Bassett and O. Sporns. Network neuroscience. *Nature neuroscience*, 20(3):353–364, 2017.

[5] H. Behjat, A. Tarun, D. Abramian, M. Larsson, and D. Van De Ville. Voxel-wise brain graphs from diffusion mri: Intrinsic eigenspace dimensionality and application to functional mri. *IEEE Open Journal of Engineering in Medicine and Biology*, 2023.

[6] T. A. Bolton and D. Van De Ville. Dynamics of brain activity captured by graph signal processing

of neuroimaging data to predict human behaviour. In *2020 IEEE 17th International Symposium on Biomedical Imaging (ISBI)*, pages 549–553. IEEE, 2020.

[7] E. Bullmore and O. Sporns. Complex brain networks: graph theoretical analysis of structural and functional systems. *Nature Reviews Neuroscience*, 10(3):186–198, 2009.

[8] E. Bullmore and O. Sporns. The economy of brain network organization. *Nature reviews neuroscience*, 13(5):336–349, 2012.

[9] L. Byrge and D. P. Kennedy. High-accuracy individual identification using a "thin slice" of the functional connectome. *Network Neuroscience*, 3(2):363–383, 2019.

[10] B. Cai, G. Zhang, A. Zhang, L. Xiao, W. Hu, J. M. Stephen, T. W. Wilson, V. D. Calhoun, and Y.-P. Wang. Functional connectome fingerprinting: identifying individuals and predicting cognitive functions via autoencoder. *Human Brain Mapping*, 42(9):2691–2705, 2021.

[11] F. R. Chung. *Spectral graph theory*, volume 92. American Mathematical Soc., 1997.

[12] J. Ciarrusta, D. Christiaens, S. P. Fitzgibbon, R. Dimitrova, J. Hutter, E. Hughes, E. Duff, A. N. Price, L. Cordero-Grande, J.-D. Tournier, et al. The developing brain structural and functional connectome fingerprint. *Developmental Cognitive Neuroscience*, 55:101117, 2022.

[13] R. R. Cruces, J. Royer, P. Herholz, S. Larivière, R. V. De Wael, C. Paquola, O. Benkarim, B.-y. Park, J. Degré-Pelletier, M. C. Nelson, et al. Micapipe: A pipeline for multimodal neuroimaging and connectome analysis. *NeuroImage*, 263:119612, 2022.

[14] S. C. de Lange, M. A. de Reus, and M. P. van den Heuvel. The laplacian spectrum of neural networks. *Frontiers in computational neuroscience*, 7:189, 2014.

[15] F. de Micheli and J. Zanelli. Quantum degenerate systems. *Journal of mathematical physics*, 53(10), 2012.

[16] G. Deco, G. Tononi, M. Boly, and M. L. Kringelbach. Rethinking segregation and integration: contributions of whole-brain modelling. *Nature Reviews Neuroscience*, 16(7):430–439, 2015.

[17] S. Deslauriers-Gauthier, M. Zucchelli, M. Frigo, and R. Deriche. A unified framework for multimodal structure-function mapping based on eigenmodes. *Medical Image Analysis*, 66:101799, 2020.

[18] V. A. Dulock and H. V. McIntosh. On the degeneracy of the two-dimensional harmonic oscillator. *American Journal of Physics*, 33(2):109–118, 1965.

[19] G. Feng, Y. Wang, W. Huang, H. Chen, J. Cheng, and N. Shu. Spatial and temporal pattern of structure-function coupling of human brain connectome with development. *bioRxiv*, pages 2023–09, 2023.

[20] E. S. Finn, X. Shen, D. Scheinost, M. D. Rosenberg, J. Huang, M. M. Chun, X. Papademetris, and R. T. Constable. Functional connectome fingerprinting: identifying individuals using patterns of brain connectivity. *Nature neuroscience*, 18(11):1664–1671, 2015.

[21] K. J. Friston. Functional integration in the brain. *Human Brain Function 2nd edn Academic Press, San Diego*, pages 971–997, 2004.

[22] A. Griffa, E. Amico, R. Liégeois, D. Van De Ville, and M. G. Preti. Brain structure-function coupling provides signatures for task decoding and individual fingerprinting. *NeuroImage*, 250:118970, 2022.

[23] W. Huang, L. Goldsberry, N. F. Wymbs, S. T. Grafton, D. S. Bassett, and A. Ribeiro. Graph frequency analysis of brain signals. *IEEE journal of selected topics in signal processing*, 10(7):1189–1203, 2016.

[24] W. Huang, T. A. Bolton, J. D. Medaglia, D. S. Bassett, A. Ribeiro, and D. Van De Ville. A graph signal processing perspective on functional brain imaging. *Proceedings of the IEEE*, 106(5):868–885, 2018.

[25] J. Irion and N. Saito. Applied and computational harmonic analysis on graphs and networks. In *Wavelets and Sparsity XVI*, volume 9597, pages 336–350. SPIE, 2015.

[26] M. Jakob and S. Stenholm. Variational functions in degenerate open quantum systems. *Physical Review A*, 69(4):042105, 2004.

[27] M. Jalbrzikowski, F. Liu, W. Foran, L. Klei, F. J. Calabro, K. Roeder, B. Devlin, and B. Luna. Functional connectome fingerprinting accuracy in youths and adults is similar when examined on the same day and 1.5-years apart. *Human brain mapping*, 41(15):4187–4199, 2020.

[28] H. Kanehisa. Degenerate modes of symmetric instability. *Journal of the Meteorological Society of Japan. Ser. II*, 86(4):557–562, 2008.

[29] K. Kumar, C. Desrosiers, K. Siddiqi, O. Colliot, and M. Toews. Fiberprint: A subject fingerprint based on sparse code pooling for white matter fiber analysis. *NeuroImage*, 158:242–259, 2017.

[30] G. Lioi, V. Gripon, A. Brahim, F. Rousseau, and N. Farrugia. Gradients of connectivity as graph fourier bases of brain activity. *Network Neuroscience*, 5(2):322–336, 2021.

[31] R. Liégeois, A. Santos, V. Matta, D. Van De Ville, and A. H. Sayed. Revisiting correlation-based functional connectivity and its relationship with structural connectivity. *Network Neuroscience*, 4(4): 1235–1251, 12 2020. ISSN 2472-1751. doi: 10.1162/netn_a_00166. URL https://doi.org/10.1162/netn_a_00166.

[32] A. I. Luppi, R. L. Carhart-Harris, L. Roseman, I. Pappas, D. K. Menon, and E. A. Stamatakis. Lsd alters dynamic integration and segregation in the human brain. *NeuroImage*, 227:117653, 2021.

[33] A. I. Luppi, J. Vohryzek, M. L. Kringelbach, P. A. Mediano, M. M. Craig, R. Adapa, R. L. Carhart-Harris, L. Roseman, I. Pappas, A. R. Peattie, et al. Distributed harmonic patterns of structure-function dependence orchestrate human consciousness. *Communications biology*, 6(1):117, 2023.

[34] M. Mantwill, M. Gell, S. Krohn, and C. Finke. Brain connectivity fingerprinting and behavioural prediction rest on distinct functional systems of the human connectome. *Communications biology*, 5 (1):261, 2022.

[35] D. S. Margulies, S. S. Ghosh, A. Goulas, M. Falkiewicz, J. M. Huntenburg, G. Langs, G. Bezgin, S. B. Eickhoff, F. X. Castellanos, M. Petrides, E. Jefferies, and J. Smallwood. Situating the default-mode network along a principal gradient of macroscale cortical organization. *Proceedings of the National Academy of Sciences*, 113(44):12574–12579, 2016.

[36] L. Marrec and S. Jalan. Analysing degeneracies in networks spectra. *Europhysics Letters*, 117(4): 48001, 2017.

[37] J. McFadden. Integrating information in the brain's em field: the cemi field theory of consciousness. *Neuroscience of Consciousness*, 2020(1):niaa016, 2020.

[38] J. D. Medaglia, W. Huang, E. A. Karuza, A. Kelkar, S. L. Thompson-Schill, A. Ribeiro, and D. S. Bassett. Functional alignment with anatomical networks is associated with cognitive flexibility. *Nature human behaviour*, 2(2):156–164, 2018.

[39] D. C. Monroe, S. L. DuBois, C. K. Rhea, and D. M. Duffy. Age-related trajectories of brain structure–function coupling in female roller derby athletes. *Brain sciences*, 12(1):22, 2021.

[40] E. J. Müller, B. R. Munn, K. M. Aquino, J. M. Shine, and P. A. Robinson. The music of the hemispheres: Cortical eigenmodes as a physical basis for large-scale brain activity and connectivity patterns. *Frontiers in Human Neuroscience*, 16:1062487, 2022.

[41] B. C. Munsell, E. Gleichgerrcht, E. Hofesmann, J. Delgaizo, C. R. McDonald, B. Marebwa, M. A. Styner, J. Fridriksson, C. Rorden, N. K. Focke, et al. Personalized connectome fingerprints: Their importance in cognition from childhood to adult years. *Neuroimage*, 221:117122, 2020.

[42] A. Ortega, P. Frossard, J. Kovačević, J. M. Moura, and P. Vandergheynst. Graph signal processing: Overview, challenges, and applications. *Proceedings of the IEEE*, 106(5):808–828, 2018.

[43] M. G. Preti and D. Van De Ville. Decoupling of brain function from structure reveals regional behavioral specialization in humans. *Nature Communications*, 10, 2019.

[44] M. G. Preti, T. A. Bolton, A. Griffa, and D. Van De Ville. Graph signal processing for neurogimaging to reveal dynamics of brain structure-function coupling. In *ICASSP 2023-2023 IEEE International Conference on Acoustics, Speech and Signal Processing (ICASSP)*, pages 1–5. IEEE, 2023.

[45] A. Raj and Y.-h. Chen. The wiring economy principle: connectivity determines anatomy in the human brain. *PloS one*, 6(9):e14832, 2011.

[46] V. Ravindra, P. Drineas, and A. Grama. Constructing compact signatures for individual fingerprinting of brain connectomes. *Frontiers in Neuroscience*, 15:549322, 2021.

[47] A. Revonsuo. Binding and the phenomenal unity of consciousness. *Consciousness and cognition*, 8 (2):173–185, 1999.

[48] J. Royer, R. Rodríguez-Cruces, S. Tavakol, S. Larivière, P. Herholz, Q. Li, R. Vos de Wael, C. Paquola, O. Benkarim, B.-y. Park, et al. An open mri dataset for multiscale neuroscience. *Scientific Data*, 9(1): 1–12, 2022.

[49] J. Rué-Queralt, V. Mancini, V. Rochas, C. Latrèche, P. J. Uhlhaas, C. M. Michel, G. Plomp, S. Eliez, and P. Hagmann. The coupling between the spatial and temporal scales of neural processes revealed by a joint time-vertex connectome spectral analysis. *NeuroImage*, 280:120337, 2023.

[50] A. Schaefer, R. Kong, E. M. Gordon, T. O. Laumann, X.-N. Zuo, A. J. Holmes, S. B. Eickhoff, and B. T. Yeo. Local-global parcellation of the human cerebral cortex from intrinsic functional connectivity mri. *Cerebral cortex*, 28(9):3095–3114, 2018.

[51] J. Sepulcre. Functional streams and cortical integration in the human brain. *The Neuroscientist*, 20(5): 499–508, 2014.

[52] J. Sepulcre. Integration of visual and motor functional streams in the human brain. *Neuroscience letters*, 567:68–73, 2014.

[53] W. H. Shaffer. Degenerate modes of vibration and perturbations in polyatomic molecules. *Reviews of Modern Physics*, 16(3-4):245, 1944.

[54] O. Sporns. Network attributes for segregation and integration in the human brain. *Current opinion in neurobiology*, 23(2):162–171, 2013.

[55] O. Sporns, D. R. Chialvo, M. Kaiser, and C. C. Hilgetag. Organization, development and function of complex brain networks. *Trends in cognitive sciences*, 8(9):418–425, 2004.

[56] G. Tononi, O. Sporns, and G. M. Edelman. A measure for brain complexity: relating functional segregation and integration in the nervous system. *Proceedings of the National Academy of Sciences*, 91(11):5033–5037, 1994.

[57] M. Ursino, C. Cuppini, and E. Magosso. Neurocomputational approaches to modelling multisensory integration in the brain: a review. *Neural Networks*, 60:141–165, 2014.

[58] D. Van De Ville, Y. Farouj, M. G. Preti, R. Liégeois, and E. Amico. When makes you unique: temporality of the human brain fingerprint. *Science advances*, 7(42):eabj0751, 2021.

[59] M. P. Van Den Heuvel and O. Sporns. Rich-club organization of the human connectome. *Journal of Neuroscience*, 31(44):15775–15786, 2011.

[60] P. Verma, S. Nagarajan, and A. Raj. Spectral graph theory of brain oscillations—-revisited and improved. *NeuroImage*, 249:118919, 2022. ISSN 1053-8119. doi: https://doi.org/10.1016/j.neuroimage.2022.118919. URL https://www.sciencedirect.com/science/article/pii/S1053811922000490.

[61] M. B. Wang, J. P. Owen, P. Mukherjee, and A. Raj. Brain network eigenmodes provide a robust and compact representation of the structural connectome in health and disease. *PLoS computational biology*, 13(6):e1005550, 2017.

[62] Xie, C. Cai, P. F. Damasceno, S. S. Nagarajan, and A. Raj. Emergence of canonical functional networks from the structural connectome. *NeuroImage*, 237:118190, 2021. ISSN 1053-8119. doi: https://doi.org/10.1016/j.neuroimage.2021.118190. URL https://www.sciencedirect.com/science/article/pii/S1053811921004675.

[63] C. Ye, J. Huang, H. Lv, J. Lu, and T. Ma. Decoupling of brain activity from connectome in multiple

sclerosis and neuromyelitis optica [abstract]. In *International Society for Magnetic Resonance in Medicine*, 2020.

[64] F.-C. Yeh, J. Vettel, A. Singh, B. Poczos, S. Grafton, K. Erickson, W.-Y. Tseng, and T. Verstynen. Local connectome fingerprinting reveals the uniqueness of individual white matter architecture. *BioRxiv*, 43778, 2016.

[65] B. T. T. Yeo, F. M. Krienen, J. Sepulcre, M. R. Sabuncu, D. Lashkari, M. Hollinshead, J. L. Roffman, J. W. Smoller, L. Zöllei, J. R. Polimeni, B. Fischl, H. Liu, and R. L. Buckner. The organization of the human cerebral cortex estimated by intrinsic functional connectivity. *Journal of neurophysiology*, 106: 1125–65, 2011. doi: 10.1152/jn.00338.2011.

[66] F. Zamani Esfahlani, J. Faskowitz, J. Slack, B. Mišić, and R. F. Betzel. Local structure-function relationships in human brain networks across the lifespan. *Nature communications*, 13(1):1–16, 2022.

[67] A. Zarkali, P. McColgan, L.-A. Leyland, A. J. Lees, G. Rees, and R. S. Weil. Organisational and neuromodulatory underpinnings of structural-functional connectivity decoupling in patients with parkinson's disease. *Communications biology*, 4(1):86, 2021.

[68] B. Zhou, X. Dou, W. Wang, H. Yao, F. Feng, P. Wang, Z. Yang, N. An, B. Liu, X. Zhang, et al. Structural and functional connectivity abnormalities of the default mode network in patients with alzheimer's disease and mild cognitive impairment within two independent datasets. *Methods*, 205: 29–38, 2022.